Electronic properties of BaCuChF (Ch=S,Se,Te) surfaces and BaCuSeF/ZnPc interfaces

Andriy Zakutayev,[1] Janet Tate,[1,a)] Heather A. S. Platt,[2] Douglas A. Keszler,[2] Corinna Hein,[3] Thomas Mayer,[3] Andreas Klein,[3] and Wolfram Jaegermann[3]
[1]*Department of Physics, Oregon State University, 301 Weniger Hall, Corvallis Oregon 97331-6507, USA*
[2]*Department of Chemistry, Oregon State University, 153 Gilbert Hall, Corvallis Oregon 97331-4003, USA*
[3]*Department of Materials and Earth Sciences, Darmstadt University of Technology, Petersenstr. 32, 64287 Darmstadt, Germany*

(Received 4 February 2010; accepted 8 March 2010; published online 20 May 2010)

BaCuChF (Ch=S,Se,Te) surfaces and BaCuSeF interfaces with zinc phthalocyanine (ZnPc) were studied by photoelectron spectroscopy. BaCuChF compounds oxidize when exposed to ambient atmosphere. Se capping layers were studied as a means to produce representative surfaces for photoelectron spectroscopic measurements. Decapped BaCuSeF surfaces remain O-free and C-free when the Se layer is evaporated but they become F-deficient. The resulting surfaces have work functions of 4.85 eV and Fermi levels located 0.25 eV above the valence band maximum. *In situ* stepwise deposition of ZnPc on a BaCuSeF film surface produced a chemically inert interface with a hole-injection barrier of 0.11 eV. © *2010 American Institute of Physics*. [doi:10.1063/1.3380594]

I. INTRODUCTION

Organic light-emitting diodes (OLEDs) and organic photovoltaic (OPV) devices commonly use In_2O_3:Sn (ITO) as a transparent anode because of its excellent transparency, high conductivity, and relatively high work function. An oxygen plasma treatment is often used to increase the work function of the anode but this process decreases the conductivity of the surface and increases its chemical reactivity, contributing to oxidation and fatigue of functional organic overlayers. To circumvent these issues, *p*-type semiconductors could be useful alternatives to ITO (an *n*-type semiconductor) as the anode in organic optoelectronic devices. In *p*-type semiconductors, the conductivity and work function can increase simultaneously. While *p*-type oxide semiconductors have been considered an attractive approach to realizing such anodes, their *p*-type doping remains quite challenging. As a result, *p*-type oxides are most often used as interlayers between *n*-type ITO and an organic film. For example, a thin NiO layer on an ITO surface leads to increased conversion efficiency of bulk heterojunction solar cells[1] and reduction in the operating voltage of organic light-emitting devices.[2]

P-type chalcogenides appear to offer distinct advantages relative to the oxides as anode materials for organic optoelectronic devices. The chalcogenides have larger conductivities than the oxides with retention of transparency and their ionization potentials can be broadly tuned based on the chalcogen, e.g., S, Se, or Te, providing a means to tune energy barriers at interfaces. Indeed, the hole injection barrier at the interface between the oxygen-plasma-treated *p*-type LaCuOSe:Mg and N,N′-diphenyl-N,N′-bis(1,1′-biphenyl)-4,4′-diamine (NPB) has already been demonstrated to be lower than the barrier at the ITO/NPB interface.[3]

Development of OLEDs and OPVs requires fundamental understanding of the properties of the interfaces. Interfaces of organic materials with metals, binary semiconductors, and transparent *n*-type semiconductors are well-studied,[4,5] however, the number of reports addressing interfaces with inorganic wide-bandgap *p*-type semiconductors is quite limited. The chalcogenides BaCuChF (Ch=S,Se,Te) comprise one such family of wide-band *p*-type semiconductors that has potential for *p*-type anode applications. Thin films of these materials are transparent through most of the visible spectrum and they have a high concentration and mobility of free holes.[6] Optical and transport properties of BaCuChF may be tuned both in powder[7] and thin-film[8] forms, which is attractive for optoelectronic applications. Another significant advantage for organic devices is that the BaCuChF materials do not contain oxygen, which may lead to better contact stability and longer device lifetime.

In this paper, we present a study of BaCuChF (Ch=S,Se,Te) surfaces using photoelectron spectroscopy (PES) and report on the interfaces between BaCuSeF and zinc phthalocyanine (ZnPc). This paper is laid out as follows. Experimental details are followed by a discussion of a new synthesis route to BaCuChF powders and pellets, including their compositional, structural, and surface characterization. Next, deposition and characterization of BaCuChF thin films are discussed with a particular emphasis on the surface preparation for the PES experiments. Finally, results of BaCuSeF/ZnPc interfacing experiments are reported.

II. EXPERIMENTS

A. Sample preparation and characterization

BaCuSF powder was synthesized by grinding $BaCO_3$ (Cerac, 99.9%), BaF_2 (Cerac, 99.9%), and Cu_2S (Strem Chemicals, 99.5%) together in stoichiometric amounts and heating in flowing H_2S (g) (Matheson, 99.5%) at 550 °C for 2 h. To prepare BaCuSeF, $BaCO_3$, and BaF_2 were ground

a)Author to whom correspondence should be addressed. Electronic mail: tate@physics.oregonstate.edu.

with Cu_2Se (Cerac, 99.5%) in stoichiometric proportions and reacted under a mixture of 15% H_2Se (g)-85% Ar (g) (Air Liquide, 99.8%) flow at 550 °C for 2 h. The gas was then switched to Ar (Industrial Welding Supply, 99%), and the powder was heated for another 2 h at the same temperature. BaCuTeF was prepared by combining $BaCO_3$, BaF_2, and Cu_2Te (Cerac, 99.5%) in stoichiometric proportions and grinding with 5–20 wt % excess Te (Alfa Aesar, 99.999%) in an Ar-filled plastic glove-bag. After grinding, the mixture was heated at 550 °C under flowing 5% H_2 and 95% Ar (Airgas, 99.999%) for 2 h.

BaCuChF powders were cold pressed at 2.7–3.6 tonnes in a 25-mm die to form targets for the pulsed laser deposition (PLD). The pellets for the photoemission experiments were pressed at 1.8 tonnes in a 9.5 mm die. BaCuSF targets and pellets were heated in a hot isostatic press (HIP, American Isostatic Presses) for 3 h under 138 MPa of Ar at 750 °C. BaCuSeF samples were treated in the HIP at 650–700 °C for 3 h with 103 MPa of Ar. BaCuTeF targets and pellets were heated for 2 h at 780 °C in the HIP with 103 MPa of Ar. Final densities were approximately 70% of theoretical values.

BaCuChF thin films were prepared by PLD in a vacuum chamber with a base pressure of 10^{-9} Torr without introducing background gas. BaCuChF sintered targets were ablated using a pulsed 1 J/cm^2 beam from a KrF excimer laser operating at a wavelength of 248 nm with a repetition rate of 7 Hz. Si (001) and amorphous silica (a-SiO_2) substrates were heated to 350 °C and rotated 5 cm above the target during the deposition. The films were 200 nm thick, as measured by a surface profilometer.

X-ray diffraction (XRD) experiments were performed using a Rigaku MiniFlex II diffractometer with Cu $K\alpha$ radiation. The resulting XRD patterns were corrected for the zero-point shift using Si peaks. Electron probe microanalysis (EPMA) on the BaCuChF pellets and films was performed using a Cameca SX-100 microprobe. Each BaCuChF pellet was sampled over several hundred microns. At least fourteen points were used to calculate the final elemental ratios of the pellets, resulting in a typical standard deviation of 2 to 4 at. %. The films were measured with three accelerating voltages (12, 16, and 22 kV). The average was taken over five points on each of the films. These data were modeled using STRATAGEM software. The absolute uncertainty of the EPMA measurements was ±5%.

Transport properties were measured for the thin films on a-SiO_2 prepared under the same conditions as the samples on Si (001) substrates. Resistivity and Hall effect were measured using a Lakeshore 7504 system in a field of 20 kG. The Seebeck coefficient was measured using a custom setup with the temperature difference of 3–5 K between hot and cold ends of the sample. Optical reflection and transmission of the samples were measured in the 200–2500 nm spectral region using an Ocean Optics visible-near infrared spectrometer.

B. PES

The PES experiments were performed using the Darmstadt Integrated System for Solar energy research.[9] Before acquiring data, the surfaces of the BaCuChF pressed pellets were polished with 1000-grit sandpaper. The polishing procedure took 5 min, and the samples were in a vacuum of 10^{-6} mbar within about 5 min of polishing.

BaCuChF thin films were protected from ambient atmosphere during transportation from Corvallis (OR), USA to Darmstadt, Germany. For this purpose, amorphous 1000-nm Se capping layers were prepared by PLD without breaking vacuum. The samples were also contained in plastic vacuum packaging during the transportation. BaCuSeF samples were decapped by heating in vacuum (10^{-8} mbar) for 10 min at 200 °C [$T_{melt}(Se)=221$ °C]. Higher temperatures increased surface nonstoichiometry, and shorter heating times left Se islands on the surface, as confirmed by EPMA. Decapping of BaCuSF and BaCuTeF samples was followed by sputter-cleaning with an additional subsequent heating for recrystallization of the surfaces. The sputter-cleaning was done by rastering a 1-μA beam of 1-keV Ar ions incident at 45° to the surfaces over a 25 mm^2 area of the sample.

X-ray-photoemission spectroscopy (XPS) and ultraviolet photoemission spectroscopy (UPS) experiments were performed in an Escalab-250 system using the $K\alpha$ line of an Al x-ray source with a monochromator (1486.6 and 0.4 eV energy resolution) and He I line from a He discharge lamp (21.2 and 0.2 eV energy resolution). During the UPS measurements, an electric potential of −6 V was applied to the samples. The Fermi level of the system was calibrated with the $3d_{5/2}$ line of a clean Ag sample (368.27 eV). XPS core level spectra were recorded over an energy range at least 10 eV larger than the full width at half maximum of each peak but only a portion of each spectrum is shown. The work function and the valence band maxima (VBM) were found from extrapolation of the linear portion of the secondary electron cut-off and the valence band (VB) onset to background level. The uncertainty of the binding energy determination was ±0.05 eV. The surface stoichiometry of the BaCuChF films was determined from the integrated area under the XPS core level peaks using sensitivity factors for the system. The absolute uncertainty of the surface composition determined this way was typically ±10%.

C. Interfacing experiments

ZnPc layers were deposited at room temperature on decapped BaCuSeF thin film surfaces by thermal evaporation of ZnPc powders heated at 393 °C. After each deposition step the samples were transferred in vacuum to the PES chamber and XPS/UPS spectra were recorded. ZnPc was deposited until the layer was thick enough that no significant changes in the binding energies of the XPS peaks of Zn, N, and C were observed.

The spectra of the BaCuSeF VB and the ZnPc highest occupied molecular orbital (HOMO) were obtained by subtracting the UPS reference spectra of the clean BaCuSeF films and that of a thick ZnPc layer from the measured BaCuSeF/ZnPc spectra for each step of the interfacing experiment. The energy differences between the UPS HOMO/VB and the XPS core levels in the reference spectra were assumed to be constant during the course of the interfacing

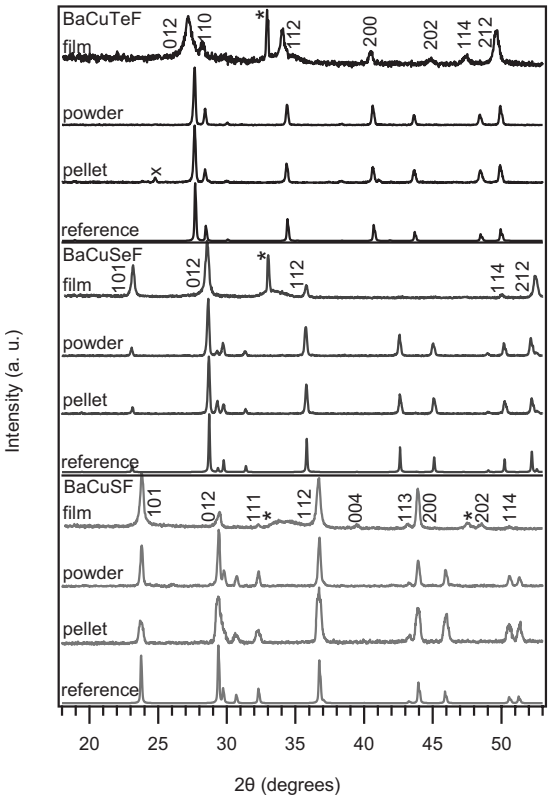

FIG. 1. BaCuChF XRD patterns of thin film, powder, pellet samples, and simulated XRD patterns. Stars denote Si substrate peaks. A cross denotes BaF_2 impurity peak.

experiment. These energy differences were used to determine the bending of the BaCuSeF VBM and ZnPc HOMO from the XPS data. Throughout this paper, we use the ZnPc HOMO maximum but the HOMO onset (0.4 eV higher) was used for the calculation of the hole injection barrier as often reported in the literature.[10,11] The hole injection barrier was calculated at 25 Å coverage, where all the ZnPc core levels started shifting in parallel.

For ZnPc thickness calculations, the area under the XPS peaks A_i was fit using expressions $A_i=A_{i0}\exp(-r_i t/d_{i0})$ for BaCuSeF peaks, and $A_i=A_{i0}[1\text{-}\exp(-r_i t/d_{i0})]$ for ZnPc peaks, where i is peak index, t is ZnPc deposition time, r_i is the deposition rate and d_i is the energy-dependent inelastic mean free path (IMFP). The IMFP of electrons in ZnPc was calculated using NIST Electron IMFP Database (v. 1.1). Deposition rates r_i extracted from these fits averaged to 0.2 Å/s, which was used to calculate the thickness of ZnPc layer for each deposition step.

III. RESULTS AND DISCUSSION

A. Powders and pellets

Syntheses of BaCuChF powders by solid state reaction between binary precursors in sealed ampoules has been previously reported[12,13] but this method led to chalcogen-poor samples with trace oxygen impurities. These problems likely result from the oxidized binary precursors, high defect concentrations in the synthesized BaCuChF powders, and subsequent oxidation of these powders when exposed to air. Flowing H_2Ch gas syntheses of the BaCuSF and BaCuSeF compounds solves these problems. At elevated temperatures, the large excess of flowing H_2Ch gas strips away oxygen and minimizes the number of Ch vacancies in the resulting BaCuChF powder:

$$BaCO_3(s) + H_2Ch(g) \rightarrow BaCh(s) + CO_2(g) + H_2O(g). \quad (1)$$

BaCuSeF powders contained excess Se and a subsequent anneal in Ar was required to remove it. H_2Te decomposes above 0 °C, so it was not possible to synthesize BaCuTeF by this method. Nevertheless, the XRD data collected from all three BaCuChF powders were consistent with the reference patterns, and no significant impurity peaks were observed (Fig. 1). Unit cell parameters calculated from the measured data are all within 0.6% of published values.[14]

EPMA data collected from the sintered BaCuChF pressed pellets are summarized in Table I. From these data, elemental ratios of BaCuSF and BaCuSeF are found to be within one standard deviation of the expected values. There is a significant excess of F with respect to each of the other elements in the BaCuTeF pellets, which is consistent with the small amount of BaF_2 observed in the XRD pattern of the BaCuTeF pellet (Fig. 1). For all three BaCuChF materials, the oxygen concentration in the pressed pellets (2%–4%) is comparable to the standard deviations in the EPMA experiments (2%–4%).

Binding energies of the XPS core levels of the BaCuChF pressed pellets are summarized in Table II. The Cu $2p_{3/2}$ and the F $1s$ binding energies in BaCuChF are close to those in Cu_2S (932.6 eV),[15] Cu_2Se (932.5 eV),[16] Cu_2Te (932.94 eV),[17] and BaF_2 (684.2 eV),[18] due to the similar crystallographic and electronic environments. Compositions measured by XPS (Table III) demonstrate that the surfaces of the BaCuSF and BaCuSeF pellets are Ba-rich, whereas the

TABLE I. Composition of BaCuChF pressed pellets (PP) and thin films (TF) measured using EPMA. Ideal stoichiemtery has each element at 25 at. % and O at 0 at. %.

EPMA (at. %)	BaCuSF		BaCuSeF		BaCuTeF	
	PP	TF	PP	TF	PP	TF
Ba	25	25	24	26	21	24
Cu	25	22	25	23	20	20
Ch	24	21	25	24	21	22
F	24	26	24	24	34	26
O	2	6	2	3	4	7

TABLE II. Binding energies (BE) of the core levels and the VB maxima of BaCuChF pellets. For the Ch atoms, S $2p_{3/2}$, Se $3d_{5/2}$, and Te $3d_{5/2}$ binding energies are reported.

BE (eV)	BaCuSF	BaCuSeF	BaCuTeF
Ba $3d_{5/2}$	779.88	779.86	780.03
Cu $2p_{3/2}$	932.53	932.50	932.80
Ch	161.15	53.51	572.11
F $1s$	684.08	684.11	684.14
VBM	0.30	0.20	0.10

TABLE III. Composition of BaCuChF pressed pellets (PP), and decapped (d) or sputter-cleaned (s) thin films (TF) measured using XPS. Ideal stoichiemtery has each element at 25 at. % and O at 0 at. %.

XPS (at. %)	BaCuSF		BaCuSeF		BaCuTeF	
	PP	TF(s)	PP	TF(d)	PP	TF(s)
Ba	25	37	26	26	21	30
Cu	14	13	17	28	12	18
Ch	17	26	13	27	23	26
F	15	16	13	16	11	19
O	27	9	30	3	30	5
C	2	0	2	0	4	0

surface of the BaCuTeF pellet is Ba-rich and Te-rich; each of the samples was found to contain approximately 30 at. % O. Oxidation results in high-binding-energy satellites for the Te $3d$ peaks [Fig. 2(a)], and a low-binding-energy component for the O $1s$ peak [Fig. 2(b)]. These features are consistent with the presence of TeO_2. TeO_2 peaks are not present in the XRD patterns of the BaCuTeF pellets (Fig. 1), indicating a thin oxide layer on the BaCuTeF surface. Similarly, the S $2p$ and Se $3d$ peaks have high-binding-energy shoulders, and the corresponding O $1s$ peaks have low-binding-energy components, indicating the presence of S–O and Se–O bonding interactions on the BaCuSF and BaCuSeF surfaces, respectively. The S-shoulders and Se-shoulders in the BaCuSF and BaCuSeF XPS spectra are much weaker than the TeO_2 peaks in the BaCuTeF spectrum, which may be rationalized by considering Gibbs free energies of different phases of Ch–O compounds. In the vicinity of the synthesis temperature (527 °C) TeO_2 exists in solid phase, whereas all S-oxides and Se oxides exist in gas phase.[19] Therefore, solid Te–O layer may form on the surfaces during the flowing gas synthesis, whereas S–O and Se–O layers may form only after the synthesis, when the samples are exposed to the atmosphere. Since the BaCuChF surfaces are Ba-rich (Table III), it is likely that Ba–O is also present at the BaCuChF surfaces. BaO satellites do not appear in the XPS, probably since the binding energies of the Ba $3d_{5/2}$ peaks in BaO and BaCuChF are very similar. Clearly, the BaCuChF grain boundaries are oxidized, and our previous electrical transport measurements are consistent with this result.[8] The BaCuChF surfaces are also contaminated with atmospheric carbon-containing molecules, which is evident from a broad C $1s$ peak at 284.58 eV [Fig. 2(c)]. A broad O $1s$ peak at

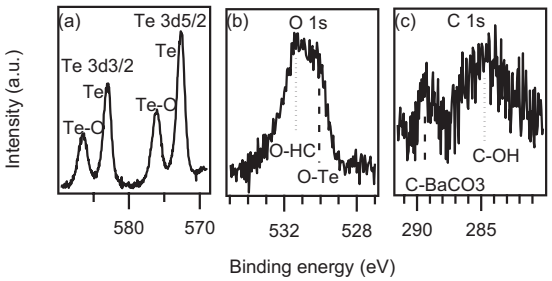

FIG. 2. X-ray photoemission spectra of Te $3d$, O $1s$, and C $1s$ core levels in BaCuTeF pressed pellets. The surfaces contain some oxygen-based and carbon-based species.

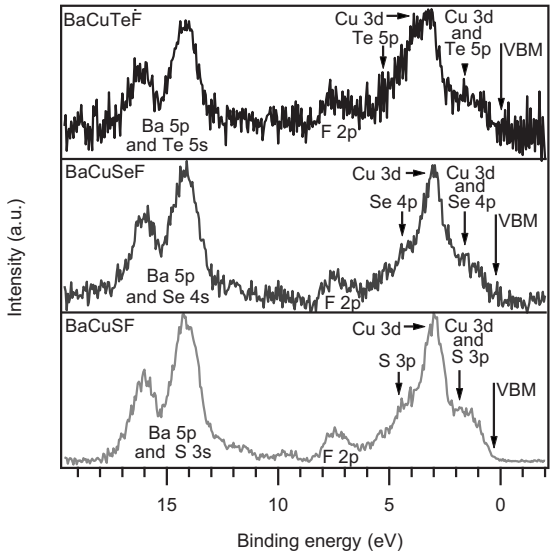

FIG. 3. X-ray photoemission spectra of the VB of BaCuChF pellets. The peaks are assigned based on DFT calculations.

531.35 eV [Fig. 2(b)] also indicates the presence of $O_xC_yH_z$ species on the surface. These two lines were not sufficiently intense to perform a deconvolution to determine their origin more precisely. A low-intensity component of the C $1s$ peak at 289.37 is consistent with the C $1s$ line in $BaCO_3$ at 289.4 eV.[20] This may be a result of using $BaCO_3$ precursors in the BaCuChF flowing-gas synthesis, or a consequence of the reaction of Ba-rich grain boundaries with atmospheric CO_2.

XPS VB spectra of all three BaCuChF are shown in Fig. 3, and the binding energies of the VBM are listed in Table II. The three VB spectra are similar to each other; their spectral features are assigned based on the partial density of states calculated using density functional theory (DFT).[13,21] Spectral positions of the peaks predicted by DFT and measured by XPS agree well but their relative intensities are not consistent with each other. For example, F $2p$ and Cu $3d$ peaks are predicted to have similar magnitude but XPS measurements indicate that the Cu $3d$ peak is much stronger (Fig. 3). This can be explained by the larger x-ray ionization cross section of d-states compared to p-states. The position of the surface Fermi level decreases across the BaCuSF–BaCuSeF–BaCuTeF series in agreement with bulk Fermi level positions trend calculated from the experimental concentration of free holes along with the DFT density of states.[22] However, the XPS results are generally higher than the theoretical prediction, which is likely caused by the bending of BaCuChF bands downward at the surface. This band bending may be result from the surface oxidation mentioned earlier. Work functions of the polished BaCuChF pellets could not be reliably determined by UPS because of the presence of atmospheric adsorbates on the surfaces.

B. Thin films

The composition of the BaCuChF thin film on Si (001) measured by EPMA is shown in Table I. All the samples are nearly stoichiometric, despite the fact that the BaCuTeF target was F-rich. We attribute the decrease in the F content in the BaCuTeF thin films largely to the low ablation efficiency

of the BaF_2 impurity because of its high band gap. The concentration of oxygen in all BaCuChF thin-film samples was higher than in the pellets, probably due to the higher surface-to-volume ratio. The films are somewhat Cu-poor. Cu vacancies likely generate free holes, leading to *p*-type nature of BaCuChF demonstrated by positive thermopower. Seebeck coefficients for the thin films on fused silica were 335 μV/K for BaCuSF, 255 μV/K for BaCuSeF, and 80 μV/K for BaCuTeF. BaCuTeF thin films on *a*-SiO_2 had a Hall mobility of 0.52 cm^2/Vs, concentration of free holes of 2.2×10^{20} cm^{-3}, resulting in a conductivity of 30 S/cm. The Hall coefficient could not be reliably determined for polycrystalline BaCuSF and BaCuSeF samples but their conductivities were 0.3 S/cm and 0.001 S/cm, respectively. thin films of 200-nm thickness were on average 75% transparent to 500–2500 nm light. Reflection-corrected transmission $T/(1-R)$ was ~90% in this spectral range.

As shown in Fig. 1, the thin films XRD patterns have no impurity peaks but they are shifted to smaller 2θ values than the powder XRD patterns, indicating larger unit cells. We attribute the unit cell expansion to the stress imposed by creation of native defects during thin films deposition. The increase in the unit cell volume is consistent with the results of the DFT defect calculation that will be published elsewhere. A similar increase in the unit cell parameters was reported for BaCuTeF thin films on fused silica[23] and $BaCu(Se_xS_{1-x})F$ thin films solid solutions on MgO.[8]

According to XPS measurements, surfaces of poorly protected BaCuChF thin films were significantly oxidized and contaminated, so it was crucial to protect them from the influence of the atmospheric conditions. Four protection methods and their combinations have been investigated, including (i) deposition of a 1000-nm selenium capping layer, (ii) sealing in a vacuum package, (iii) direct transfer from the loadlock into a nitrogen-filled glove-bag for sealing, and (iv) storage in nitrogen atmosphere during the transportation. After a two-week storage, only the films that were protected with the Se capping layer and sealed in a vacuum package were largely free of surface oxide. The concentration of oxygen on the surface of these samples measured by XPS (Table III) was close to the concentration of oxygen in the bulk measured by EPMA (Table I). These results demonstrate that a 1000-nm Se capping layer provides sufficient protection for short periods of atmospheric exposure; similar findings have been reported for $CuInSe_2$ thin films.[24]

In the case of the BaCuSeF thin films, evaporation was sufficient to remove the Se capping layer from the surface but decapped BaCuSeF thin films surfaces were F-poor. These films exhibited a Fermi level positioned 0.25 eV above the VBM, a work function of 4.85 eV, and a resulting ionization potential of 5.10 eV. This is an average ionization potential because BaCuSeF thin films were polycrystalline. BaCuSeF pressed pellets reported previously had a similar Fermi level (0.3 eV) but lower work function (3.6 eV) and ionization potential (3.9 eV).[21] These differences are larger than experimental uncertainties and may result from different magnitudes of surface dipoles caused by different synthesis routes, different types of samples and different surface preparation protocols. Larger surface roughness of the pressed pellets compared to thin films may also contribute to smaller work functions of the pellets. Regardless of the reason, the BaCuSeF ionization potentials reported here and previously are smaller than those of related $Cu_{2-x}Se$ (5.35 eV) (Ref. 25) and $CuInSe_2$ (5.65–6.10 eV).[26,27] The difference in ionization potentials between BaCuSeF and other Cu–Se-based materials may also be caused by the upward VB shift associated with the transfer of charge from Ba–F layers to the Cu–Se layers in the aniosotropic BaCuSeF structure. The ionization potential of BaCuSeF is larger compared to BaSe (4.7 eV),[28] as expected from more ionic nature of BaSe. The anisotropic layered crystal structure of BaCuSeF also results in polar surfaces, which may lead to a reconstruction and change the ionization potential of BaCuSeF.

In the cases of BaCuTeF and BaCuSF thin films, no heating conditions were found to completely remove the Se capping layer. Sputter-cleaning removed most of the residual Se but changed the shape of Cu LMM Auger line and resulted in preferential removal of light Cu and F atoms. Subsequent heating restored the expected shape of Cu LMM line but it did not significantly change the surface composition (Table III). Resulting low work functions (3.2–3.5 eV) are not intrinsic for BaCuSF and BaCuTeF because the surfaces of the samples were destroyed by the sputter-cleaning, as confirmed by low work functions of sputtered BaCuSeF surfaces. From these results, we conclude that capping and subsequent removal of S and Te layers should be a better way to prepare representative BaCuSF and BaCuTeF surfaces.

C. Interfaces

Metal phthalocyanines (ZnPc, CuPc, NiPc, *etc.*) are used in optoelectronic devices, often in direct contact with the anode.[10,29] We chose ZnPc for the interfacing experiments, because ITO/ZnPc interfaces have already been studied by XPS,[10] and these experiments provide good comparisons for the present work. CuPc is more commonly used in OLEDs but using ZnPc prevents interference of the XPS Cu core level signals from CuPc and BaCuChF. Since the HOMO of CuPc and ZnPc and the VB of $Cu_{1.7}Se$ and BaCuSeF have similar character,[21,30] published $Cu_{1.7}Se$/CuPc UPS interfacing experiments[11] may be also compared to this work.

Stepwise deposition of ZnPc on the decapped BaCuSeF surfaces resulted in intensity attenuation of the BaCuSeF spectra along with increase in intensity of the ZnPc spectra. Normalized area under the BaCuSeF XPS peaks, and one minus normalized area under the ZnPc XPS peaks, are shown in Figs. 4(a) and 4(b) as a function of ZnPc deposition time. The high-binding-energy peaks change intensity faster than the low-binding-energy peaks, which is consistent with the energy dependence of the IMFP of photoelectrons in ZnPc [Fig. 4(c)]. This consistency indicates that there is no interdiffusion at the BaCuSeF/ZnPc interface.

As shown in Fig. 5, the photoemission spectra shift as the BaCuSeF/ZnPc interface is formed but their shapes do not change. The area under all core level spectra was normalized to 1 to make the shapes of the spectra more evident. No chemical reaction occurs at the BaCuSeF/ZnPc interface because the C 1*s* peak has a characteristic line shape with

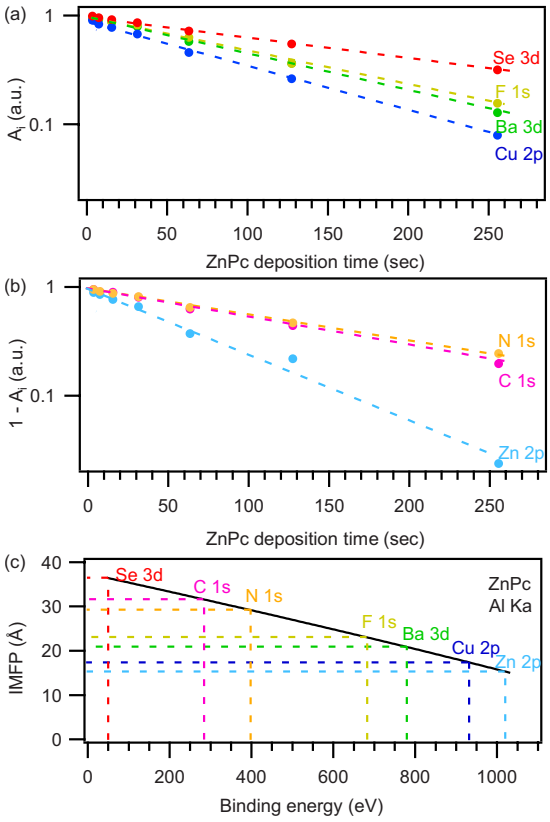

FIG. 4. (Color online) (a) Normalized area under the BaCuSeF XPS and (b) one minus normalized area under the ZnPc XPS peaks. (c) Inelastic mean free path (IMFP) of photoelectrons in ZnPc as a function of their binding energy for Al $K\alpha$ excitation radiation. Dashed color-coded lines are guides for the eye.

three components for all ZnPc thicknesses.[31] The spectral positions of the XPS core level peaks of a thick ZnPc layer (1022.43 eV for Zn $2p_{3/2}$, 398.99 eV for N 1*s*, and 284.76 eV for C 1*s* lines), its UPS HOMO binding energy (1.1 eV), and its work function (4.15 eV) all favorably agree with typical values reported in the literature for this material.[32,33] The BaCuSeF thin films spectra also do not show any evidence of a chemical reaction and the XPS binding energies (Fig. 5) are consistent with those of the pellets (Table II).

The shift in the ZnPc XPS peaks with increasing thickness of the ZnPc layer is caused by a charge transfer. Starting from a thick ZnPc layer and moving toward the interface, the XPS core levels and UPS HOMO of ZnPc shift, in parallel, to lower binding energies, over the range of 100–1000 Å depending on the preparation of the BaCuSeF surface. Since no shift in the BaCuSeF electronic states is observed (Fig. 5), the charge transfer must occur to BaCuSeF surface states. The electrons transfer from N and C atoms because the HOMO and 1*s* spectra of N and C shift to a higher binding energy at a ZnPc coverage of less than 25 Å. Zn states do not contribute to the HOMO of ZnPc, thus the Zn $2p_{3/2}$ core level shifts to a lower energy below 25 Å. The secondary electron edge shifts to a higher binding energy with increasing ZnPc thickness, which corresponds to a lowering of the work function and to the proposed direction of the charge transfer. The summary of the changes in the binding energies and the work functions discussed above are shown in Fig. 6. We conclude that the transfer of valence electrons from individual ZnPc molecules into BaCuSeF surface traps leads to a nonparallel shift in the ZnPc electronic states, causes the

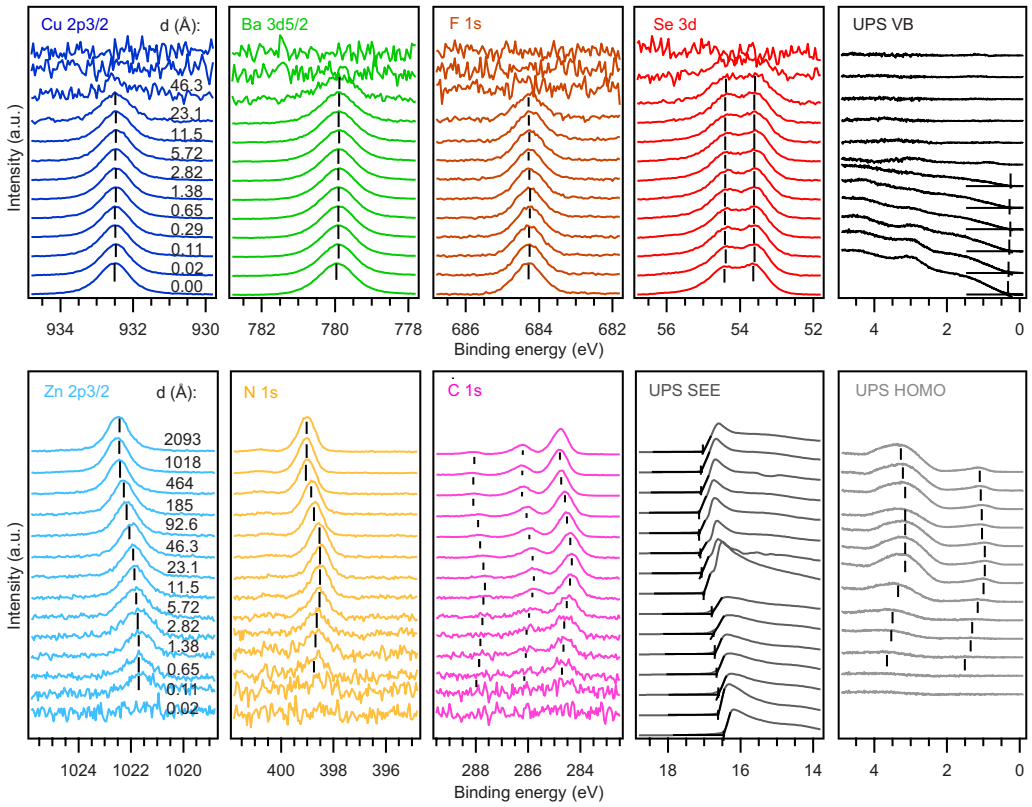

FIG. 5. (Color online) Photoemission spectra of BaCuSeF and ZnPc for different steps of the interfacing experiment. ZnPc thicknesses indicated in the first panel are the same for all other panels in a row. The vertical lines indicate binding energies used to plot Fig. 6. The color-coding is the same as in Fig. 4.

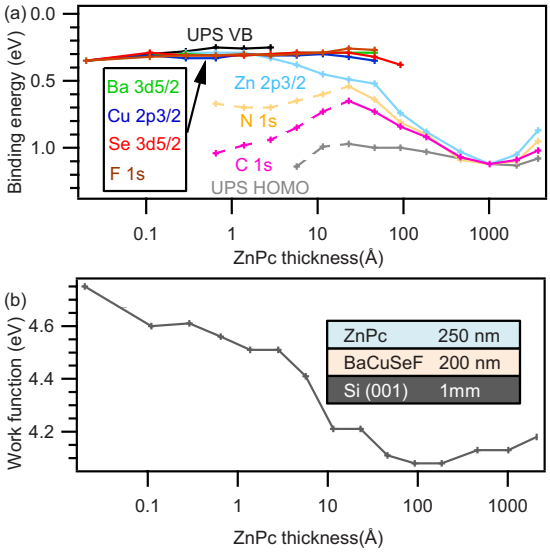

FIG. 6. (Color online) (a) Binding energy of the VB of BaCuSeF and the HOMO of ZnPc measured by UPS and determined from different XPS core level spectra. (b) Work function of the BaCuSeF/ZnPc interface. Color-coded lines are guides for the eye and the dashed portion of the N, C, and HOMO lines below 25 Å represents the charge transfer shift. Note that the abscissa is logarithmic. The final configuration of the sample is schematically depicted in the inset.

change in the work function for coverage less than 25 Å, and results in an upward bending of the ZnPc states towards the interface.

A detailed BaCuSeF/ZnPc band alignment diagram is presented in Fig. 7. The right-hand side (ZnPc side) of the diagram was plotted using averages of the data shown in Fig. 6. The left-hand side (BaCuChF side) consists of only two data points, "surface" (measured by XPS/UPS) and "bulk" (calculated from the BaCuSeF density of states and the carrier concentration),[22] so the horizontal axis on the left-hand side in Fig. 6 is arbitrary. An offset between the conduction band of BaCuSeF and the lowest unoccupied molecular orbital (LUMO) of ZnPc was calculated using the BaCuSeF band gap value found in literature[22] and the ZnPc

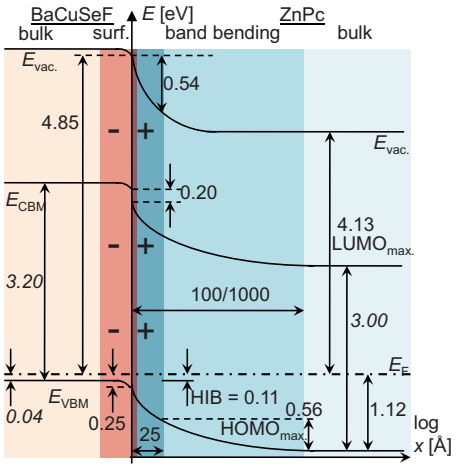

FIG. 7. (Color online) BaCuSeF/ZnPc band diagram. The VBM/HOMO and the vacuum level alignments are found from the data in Fig. 6. The band gap values are taken from literature. The bulk Fermi level of BaCuSeF is calculated from the DFT density of states and the concentration of free holes. Note that the abscissa is logarithmic.

HOMO-LUMO energy difference as measured by PES and inverse PES on gold.[32] The hole injection barrier, found as the binding energy of the ZnPc HOMO onset at 25 Å coverage is only 0.11 eV. This barrier is lower than at the ITO/ZnPc interface[10] and at the oxygen plasma treated $Cu_{1.7}Se$/CuPc interface.[11] The alignment of BaCuSeF bands with ZnPc states is favorable for efficient hole extraction in photovoltaic devices. Therefore BaCuSeF may be a better anode for OLEDs and OPV devices than ITO and $Cu_{1.7}Se$. We believe that the low hole injection barrier and favorable band alignment is due to the absence of excess oxygen at the BaCuSeF/ZnPc interface. A similar result should be possible with other *p*-type Cu–Se-based materials but only if their surfaces are protected from oxidation.

IV. SUMMARY

BaCuChF (Ch=S,Se,Te) powders synthesized from $BaCO_3$ precursors exhibit improved stoichiometries relative to similar powders synthesized by other routes. According to XPS measurements, the surfaces of BaCuChF pellets are oxidized upon exposure to atmospheric conditions. Deposition of a Se capping layer effectively limits this oxidation for BaCuSeF thin films. Decapped BaCuSeF surfaces are free of O and C, F-poor, and have work functions of 4.85 eV. The BaCuSeF/ZnPc interface is chemically inert, exhibiting a hole injection barrier of 0.11 eV. These properties should afford improved device performance for OLEDs and OPVs in comparison to those achieved with ITO and $Cu_{1.7}Se$ electrodes. thin films deposition and interface fabrication must be carefully controlled for oxygen incorporation to realize optimum performance.

ACKNOWLEDGMENTS

This work was supported by the Deutsche Forschungsgemeinschaft (Germany) within the framework of the collaborative research center SFB 595 and by the National Science Foundation (USA) under Grant No. DMR-0804916. We thank D. Wöhrle (Bremen, Germany) for providing purified ZnPc powders. We also thank Joshua Russell and David H. McIntyre for their assistance with the optical spectroscopy measurements.

[1]M. D. Irwin, D. B. Buchholz, A. W. Hains, R. P. H. Chang, and T. J. Marks, Proc. Natl. Acad. Sci. U.S.A. **105**, 2783 (2008).
[2]S. Tokito, K. Noda, and Y. Taga, J. Phys. D **29**, 2750 (1996).
[3]H. Yanagi, M. Kikuchi, K.-B. Kim, H. Hiramatsu, T. Kamiya, M. Hirano, and H. Hosono, Org. Electron. **9**, 890 (2008).
[4]J. C. Scott, J. Vac. Sci. Technol. A **21**, 521 (2003).
[5]N. Papageorgiou, E. Salomon, T. Angot, J.-M. Layet, L. Giovanelli, and G. L. Lay, Prog. Surf. Sci. **77**, 139 (2004).
[6]J. Tate, P. F. Newhouse, R. Kykyneshi, P. A. Hersh, J. Kinney, D. H. McIntyre, and D. A. Keszler, Thin Solid Films **516**, 5795 (2008).
[7]C.-H. Park, D. A. Keszler, H. Yanagi, and J. Tate, Thin Solid Films **445**, 288 (2003).
[8]A. Zakutayev, D. H. McIntyre, G. Schneider, D. A. Keszler, C.-H. Park, and J. Tate, "Tunable properties of wide-bandgap *p*-type BaCu$(Ch_{1-x}Ch'_x)F$ (Ch=S, Se, Te)," Thin Solid Films (in press).
[9]J. Fritsche, A. Klein, and W. Jaegermann, Adv. Eng. Mater. **7**, 914 (2005).
[10]Y. Gassenbauer and A. Klein, J. Phys. Chem. B **110**, 4793 (2006).

[11]H. Hiramatsu, I. Koizumi, K.-B. Kim, H. Yanagi, T. Kamiya, M. Hirano, N. Matsunami, and H. Hosono, J. Appl. Phys. **104**, 113723 (2008).
[12]H. Yanagi, J. Tate, S. Park, C.-H. Park, and D. A. Keszler, Appl. Phys. Lett. **82**, 2814 (2003).
[13]C.-H. Park, R. Kykyneshi, A. Yokochi, J. Tate, and D. A. Keszler, J. Solid State Chem. **180**, 1672 (2007).
[14]W. J. Zhu, Y. Z. Huang, F. Wu, C. Dong, H. Chen, and Z. X. Zhao, Mater. Res. Bull. **29**, 505 (1994).
[15]D. Brion, Appl. Surf. Sci. **5**, 133 (1980).
[16]D. Cahen, P. J. Ireland, L. L. Kazmerski, and F. A. Thiel, J. Appl. Phys. **57**, 4761 (1985).
[17]B. Späth, K. Lakus-Wollny, J. Fritsche, C. S. Ferekides, A. Klein, and W. Jaegermann, Thin Solid Films **515**, 6172 (2007).
[18]A. Gauzzi, H. J. Mathieu, J. H. James, and B. Kellett, Vacuum **41**, 870 (1990).
[19]I. Barin, F. Sauert, E. Schultze-Rhonhof, and W. Shu Sheng, *Thermochemical Data of Pure Substances* (VCH, New York, 1993).
[20]A. B. Christie, J. Lee, I. Sutherland, and J. M. Walls, Appl. Surf. Sci. **15**, 224 (1983).
[21]H. Yanagi, J. Tate, S. Park, C.-H. Park, D. A. Keszler, M. Hirano, and H. Hosono, J. Appl. Phys. **100**, 083705 (2006).
[22]A. Zakutayev, R. Kykyneshi, G. Schneider, D. H. McIntyre, and J. Tate, Phys. Rev. B. 81, 155103 (2010).
[23]R. Kykyneshi, D. H. McIntyre, J. Tate, C.-H. Park, and D. A. Keszler, Solid State Sci. **10**, 921 (2008).
[24]T. Schulmeyer, R. Hunger, A. Klein, W. Jaegermann, and S. Niki, Appl. Phys. Lett. **84**, 3067 (2004).
[25]D. Fuertes Marrón, T. Glatzel, A. Meeder, T. Schedel-Niedrig, S. Sadewasser, and M. C. Lux-Steiner, Appl. Phys. Lett. **85**, 3755 (2004).
[26]S. Siebentritt and U. Rau, *Wide-Gap Chalcopyrites* (Springer, Berlin, 2006).
[27]T. Schulmeyer, Ph.D. thesis, Technische Universität Darmstadt, 2005.
[28]R. J. Zollweg, Phys. Rev. **111**, 113 (1958).
[29]L. S. Hung and C. H. Chen, Mater. Sci. Eng., R. **39**, 143 (2002).
[30]Z. Liu, X. Zhang, Y. Zhang, and J. Jiang, Spectrochim. Acta, Part A **67**, 1232 (2007).
[31]H. Peisert, M. Knupfer, T. Schwieger, and J. Fink, Appl. Phys. Lett. **80**, 2916 (2002).
[32]U. Weiler, T. Mayer, W. Jaegermann, C. Kelting, D. Schlettwein, S. Makarov, and D. Wöhrle, J. Phys. Chem. B **108**, 19398 (2004).
[33]A. Kahn, N. Koch, and W. Gao, J. Polym. Sci., Part B: Polym. Phys. **41**, 2529 (2003).